



A numerical investigation of 3-D flow regimes in a toroidal natural convection loop

El Hassan Ridouane^a, Darren L. Hitt^b, Christopher M. Danforth^{a,c,*}

^aDepartment of Mathematics & Statistics, University of Vermont, 16 Colchester Ave., Burlington, VT 05405, USA

^bMechanical Engineering Program, School of Engineering, 33 Colchester Ave., University of Vermont, Burlington, VT 05405, USA

^cComplex Systems Center, Vermont Advanced Computing Center, University of Vermont, Burlington, VT 05405, USA

ARTICLE INFO

Article history:

Received 3 November 2010

Accepted 16 March 2011

Available online 6 September 2011

Keywords:

Unsteady natural convection

Thermosyphon

3-D numerical simulations

Chaotic regime

Power spectrum

ABSTRACT

Transient laminar natural convection regimes occurring in a thermal convection loop heated from below and cooled from above are investigated numerically for a wide range of Rayleigh numbers spanning the interval from 10^3 to 2.6×10^7 . In the model system, the lower half of the loop is heated and maintained at a constant high temperature, while the upper half is cooled and maintained at a constant low temperature. A three-dimensional numerical model based on the finite volume method is used to solve the system of governing flow equations. Simulations are performed using water as the working fluid ($Pr = 5.83$) and detailed numerical results are presented and discussed for conduction, steady convection, and unsteady flow regimes. Although this subject has attracted researchers for decades, there have been no detailed three-dimensional numerical simulations of the dynamics of flow in the thermal convection loop. The objective of the present study is to fill this gap by presenting the temporal evolution of the velocity and temperature fields at key locations within the system. Emphasis is given to the analysis of dynamical behavior of the flow during the unsteady regime. The complexity of flow in the loop, which is characterized by vertical structures and flow recirculation, is visualized for the first time by performing detailed 3-D numerical simulations.

© 2011 Elsevier Ltd. All rights reserved.

1. Introduction

Many phenomena of interest to the geophysical community are driven by natural convective flow (e.g. mesoscale convective thunderstorms). In fact, initial efforts to demonstrate the chaotic nature of the Earth's atmosphere were undertaken through numerical studies of the deterministic, non-periodic flow observed in a low-dimensional model of Rayleigh–Bénard convection [9]. Indeed, mathematical methods designed to improve the predictability of operational weather forecast models (e.g. ensemble forecasting) typically undergo a series of trials on increasingly complex flows, invariably including an initial audition with the 1963 Lorenz model. Constraining the spatial geometry even further, thermal convection loops (also known as “thermosyphons”) force convection to occur in a single large cell, and represent potentially the simplest physical realization of deterministic, non-periodic fluid flow.

As noted in the early reviews by Mertol and Greif [1] and by Greif [2], the flow in natural convection loops continues to be an area of considerable interest in engineering, geophysics and environmental sciences. The review articles [1,2] contain a wealth of literature on theoretical and experimental studies of this simple

system, which exhibits typical nonlinear convective effects [3,4]. However, a detailed literature survey identified only a very limited number of numerical studies of natural convection loops.

Lavine et al. [5,6] reported the outcome of a three-dimensional study of natural convection, assuming steady-state conditions, and flow symmetry about the vertical plane. In this work, the bottom half of the loop is heated at a constant heat flux, and the top half is cooled at a constant temperature. The differential equations written in their elliptic form were solved using a finite difference method. The study was undertaken in two distinct parts. In the first part [5], the Grashof number was fixed at 1900 and the effect of a tilted angle varying between 0° and 90° was investigated. It was shown that the flow is strongly three-dimensional and that the 3-D flow structure increased the flow resistance. Regions of streamwise flow reversals were predicted for a low tilt angle causing the total buoyancy to decrease. In the second part [6], results were presented for two different Grashof numbers and exhibited flow behavior which had been experimentally observed at higher Grashof numbers including flow reversals and secondary motions. The strength of these flows was found to increase at higher Grashof numbers whereas the total buoyancy decreased. Burroughs et al. [7] numerically analyzed the flow in the loop at low Grashof number for a wide range of Prandtl numbers using a Fourier–Chebyshev spectral method. Assuming that the flow is two-dimensional, Desrayaud et al. [8] investigated, numerically, the unsteady

* Corresponding author at: Department of Mathematics & Statistics, University of Vermont, 16 Colchester Ave., Burlington, VT 05405, USA. Tel.: +1 802 656 3062.

E-mail address: chris.danforth@uvm.edu (C.M. Danforth).

Nomenclature

| | | | |
|-----------|--|----------------------|--|
| c_p | specific isobaric heat capacity, J/kg K | T_0 | reference temperature, $[= (T_H + T_C)/2]$, K |
| d | diameter of the cross-section of the loop, $[= r_o - r_i]$, m | u | velocity vector, m/s |
| e | specific energy | V | velocity magnitude, m/s |
| g | acceleration of gravity, m/s^2 | <i>Greek letters</i> | |
| h | mean convective coefficient, $W/m^2 K$ | α | thermal diffusivity, $[= k/\rho c_p]$, m^2/s |
| k | thermal conductivity, $W/m K$ | β | coefficient of volumetric thermal expansion, $1/K$ |
| \dot{m} | mass flow rate, kg/s | μ | viscosity, kg/m s |
| Nu | mean Nusselt number, $[= hd/k]$ | ν | kinematic viscosity, $[= \mu/\rho]$, m^2/s |
| p | static pressure, Pa | ρ | density, kg/m^3 |
| Pr | Prandtl number, $[= \nu/\alpha]$ | τ | Newtonian viscous stress tensor |
| Q | heat transfer rate, W | <i>Subscripts</i> | |
| r_i | inner radius, m | C | cold wall |
| r_o | outer radius, m | H | hot wall |
| R | radius ratio, $[= (r_o + r_i)/d]$ | max | maximum value |
| Ra | Rayleigh number, $[= g\beta(T_H - T_C)d^3/\nu\alpha]$ | | |
| t | time, s | | |
| T | temperature, K | | |

laminar natural convection in a loop subject to a constant heat flux over the bottom half and maintained at a constant temperature over the top half. Results of a parametric study varying Ra and Pr were obtained for the case of a relatively thick loop (radius ratio $R = 3$). In summary, it has been demonstrated that the flow complexity reported in previous experimental studies can be reproduced in numerical simulations: namely regimes characterized by a steady flow, periodic flow and Lorenz-like chaotic flow [9].

Stability analyses play a key role in interpreting and understanding the dynamics of the flow within a thermal convection loop. An experimental study of natural convection was reported by Creveling et al. [4] for a glass loop filled with water and oriented in a vertical plane. At low heat transfer rates and also at high heat transfer rates the flow was observed to be steady. For an intermediate range of heating, however, the flow was found to be highly oscillatory. Their experimental observations agreed with the theoretical analyses by Keller [10] and Welander [3]. Gorman et al. [11] presented a quantitative comparison of the flow in a natural convection loop with the nonlinear dynamics of the Lorenz model. Their model featured a constant heat flux over the bottom half and isothermal cooling over the top half. The boundaries of different flow regimes were determined experimentally and the characteristics of chaotic flow regimes were discussed. They also derived a relationship between the parameters of the Lorenz model and the experimental parameters of the fluid and loop.

In a combined theoretical and experimental investigation, Yuen and Bau [12] used optimal control theory to construct a controller to suppress chaotic flow regimes in a natural convection loop. This technique is often used in many industrial processes to maintain desirable flow conditions. The authors demonstrated, in both experiments and theory, that the nature of the flow in a loop heated from below and cooled from above can be significantly modified and that chaos can be controlled. Tang and Bau [13–17] studied analytically and experimentally the stabilization of the flow in Rayleigh–Bénard convection using feedback controllers. With the aid of a controller, they showed that the transition from no-motion to steady convection can be significantly postponed.

The stability of single-phase loops has also been the subject of investigation by Vijayan and Austregesilo [18]. Scaling laws were developed and successfully verified against experimental data using various loop geometries. The stability behavior of uniform diameter loops can be expressed in terms of non-loop dimensionless groups of parameters. These correlations have recently been extended to loops with non-uniform diameters by Vijayan [19]. Jiang et al. [20] studied the effects of boundary conditions on flow stabil-

ity in a natural convection loop. The experiment was performed on a copper torus and the observations were in contrast with those reported on a glass torus. The Lorenz-like chaotic flow was not observed and the authors attributed this to the fact that the high thermal conductivity of the walls deforms the heat flux distribution and hence affects the global flow stability. Jiang and Shoji [21] also focused their study on the influence of thermal boundary conditions on the spatial and temporal stabilities of the flow. Multi-scale analysis was applied to study the flow fluctuation and self-organization in a thermal convection loop. In the analysis, a coefficient was proposed to measure the differences in thermal boundary condition. Depending on the value of this coefficient, spatial and/or temporal instabilities may occur leading to Lorenz-like or intermittent chaos. More recently, Ridouane et al. [22] numerically studied the chaotic flow in a 2-D thermal convection loop driven by hot and cold isothermal boundaries on the bottom and top halves of the loop, respectively. Detailed numerical simulations of the transitions taking place as the flow reverses direction during the chaotic regime were revealed for the first time by presenting the temporal evolution of the flow structure during these transitions. The reversal onset was characterized by deformations taking the form of small circulations propagating along the wall away from the discontinuity and against the new direction of rotation, while new cells with higher intensity were created at the discontinuity. This behavior, which

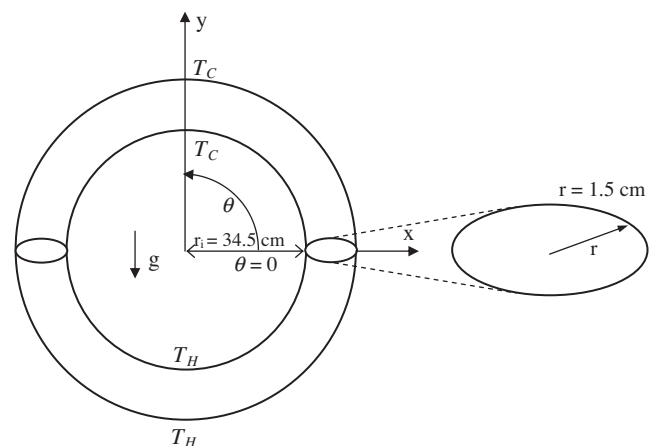


Fig. 1. Schematic diagram of the model system (not drawn to scale). The exterior of the lower half is heated and maintained at a constant high temperature T_H , while the exterior of the upper half is cooled at a constant low temperature T_C .

Table 1

Grid independence study at $Ra = 1.5 \times 10^5$. The optimal computational grid is constructed with 1,784,139 finite volume tetrahedral elements. Grid independence was achieved within one percent of the maximum velocity magnitude, the mass flow rate as well as the heat transfer rate at the walls.

| Mesh | V_{max} (m/s) | Q_H (W) | Q_C (W) | \dot{m} (kg/s) |
|-----------|-----------------------|-----------|-----------|------------------|
| 350,000 | 6.71×10^{-3} | 99.02 | -99.02 | 0.00129 |
| 905,355 | 7.09×10^{-3} | 107.55 | -107.55 | 0.00132 |
| 1,784,139 | 7.28×10^{-3} | 103.65 | -103.65 | 0.00135 |
| 3,623,000 | 7.35×10^{-3} | 102.87 | -102.87 | 0.00136 |

resembles the well-known Kelvin–Helmholtz instability, intensified with time after the fluid velocities had dropped significantly.

The present study involves the 3-D unsteady numerical simulation of laminar natural convection in a “slender” toroidal loop wherein the torus radius is much larger than the pipe radius ($R = 24$). No assumptions are made with regard to midplane symmetry, thus allowing for the possibility of fully three-dimensional flow structures. Particular care is devoted to two aspects: (1) to determine the existing flow regimes that can be encountered as the Rayleigh number increased from 10^3 to 2.6×10^7 and (2) to delineate the temporal changes triggered by the flow structures. The body of the paper is divided in two sections. The physical system and the mathematical formulations are addressed in the first section. The second section presents a discussion of the temporal evolution of the velocity and temperature fields. Particular empha-

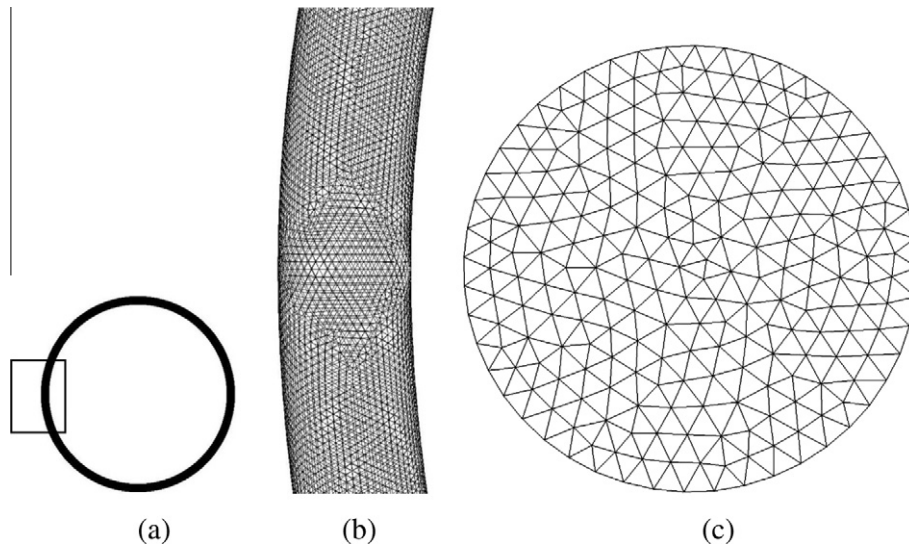


Fig. 2. Details of the computational grid illustrating the distribution of elements within the domain: (a) schematic of the loop (b) side view of the left region between the hot and cold walls as marked in (a) and (c) cross-section view. The mesh is constructed with 1,784,139 tetrahedral elements.

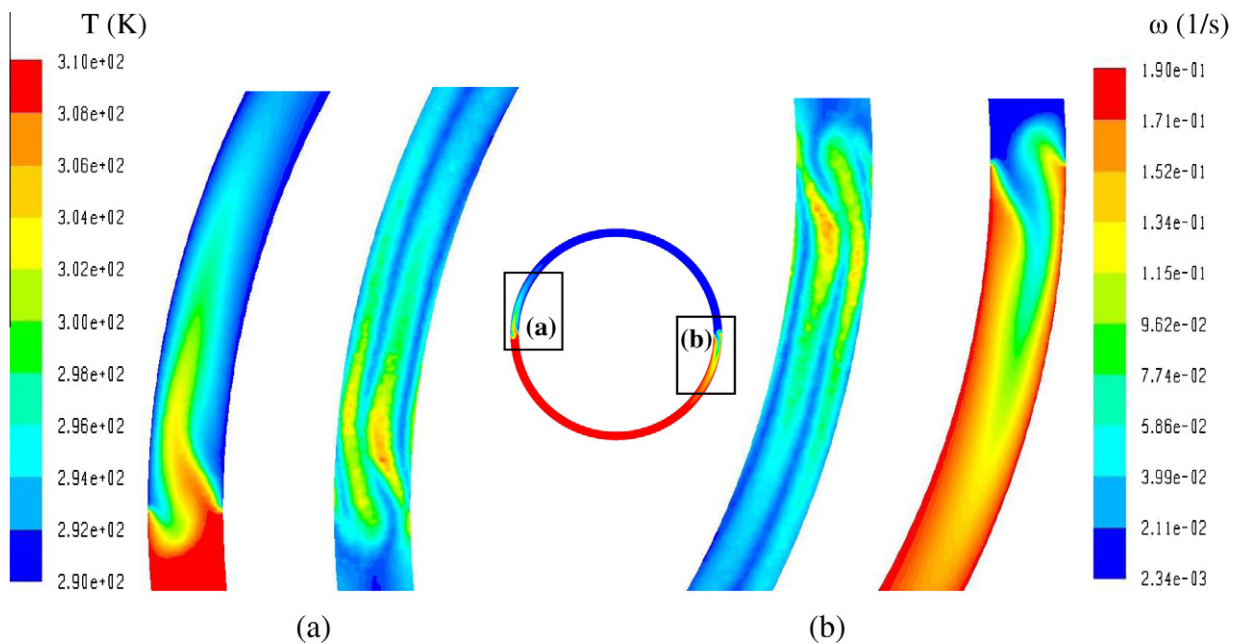


Fig. 3. Distributions of temperature (left) and vorticity (right) on the vertical mid-plane at Ra of 25,000. The fluid motion is very slow and consists of small counter rotating cells. The circulations are limited to the regions where the temperature discontinuity occurs and the remaining fluid along the loop is motionless (indicated as regions (a) and (b) in the figure).

sis is placed on flow patterns during the unsteady convection regime at high values of the Rayleigh number.

2. Computational methods

The physical system for this problem, depicted schematically in Fig. 1, consists of a circular loop filled with water and oriented in a vertical plane. The physical dimensions of the loop are 69 cm inner diameter and 75 cm outer diameter, giving a radius ratio R of 24. Initially the water is in thermal equilibrium at $T_0 = 300$ K. To initiate natural convection airflow in the closed space, the lower ($\theta = \pi$ to 2π) walls are heated and maintained at a high temperature $T_H = 310$ K while the upper ($\theta = 0$ to π) walls are cooled and maintained at a low temperature $T_C = 290$ K. In all numerical results presented, a constant temperature differential ($T_H - T_C$) of 20 K is maintained between the hot and cold walls. Variations in the Rayleigh number are achieved by adjusting the value of the gravitational acceleration, this modest temperature differential, the standard Boussinesq approximation is invoked and all thermo-physical properties – save density – are assumed to be constant and evaluated at the reference temperature T_0 . This approximation can be justified numerically by allowing these properties to vary linearly with temperature: the results demonstrate negligible impact on the flow. Additionally, the viscous dissipation is neglected due to low velocities. Under these assumptions, the governing equations are the unsteady, 3-D laminar Navier–Stokes equations along with the energy equation:

$$\frac{\partial \rho}{\partial t} + \nabla \cdot (\rho u) = 0, \quad (1)$$

$$\frac{\partial (\rho u)}{\partial t} + \nabla \cdot (\rho u u) = -\nabla p + \rho(T)g + \nabla \cdot \tau, \quad (2)$$

$$\frac{\partial e}{\partial t} + \nabla \cdot (\rho u e) = \nabla \cdot (k \nabla T), \quad (3)$$

$$e = c_p T + \frac{1}{2} |u|^2, \quad (4)$$

$$\rho(T) = \rho_0 (1 + \beta(T - T_0)), \quad (5)$$

where τ is assumed to be the Newtonian viscous stress tensor. No slip velocity boundary conditions are imposed on the walls. Prescribed isothermal boundary conditions of T_H and T_C are imposed on the heated and cooled lower and upper walls, respectively.

The governing equations are solved numerically using the finite volume method (software FLUENT 6.3 [23]). An implicit segregated solver is used and all discretization schemes employed are of second-order accuracy or higher. The QUICK scheme is used for the momentum, energy and density discretization. A second-order body-force-weighted scheme is used in the pressure discretization and the SIMPLE scheme is used in the pressure–velocity coupling. Convergence of a simulation at each time step was assessed through the monitoring of computed residuals (velocity, energy and mass conservation) and also through the convergence of point and/or surface monitors for velocity, temperature, and heat flux at selected locations in the domain by setting their absolute convergence criterion to 10^{-6} . This numerical approach has been successfully used in a previous study on the 2-D natural convection loop [22]. In this study, numerical simulations are performed using water as a working fluid ($Pr = 5.83$) and for Rayleigh numbers varying from 10^3 to 2.6×10^7 .

To ensure the numerical results were independent of the three-dimensional grid resolution, a formal grid sensitivity study was performed. Grid sizes ranging from 350,000 to 3,623,000 tetrahedral elements were examined in the steady-state convection regime at $Ra = 1.5 \times 10^5$. Grid independence was achieved within one percent with the uniform grid size of 1,784,139 tetrahedral elements. Table 1 illustrates the effect of the grid size on the solu-

tion. Details of the computational grid employed in this study are shown in Fig. 2. The numerical approach used was successfully verified in the previous 2-D study conducted by the authors [22].

3. Results and discussion

For the problem of the thermal convection loop it has been demonstrated both theoretically and experimentally that multiple flow regimes are possible. Depending on the value of the Rayleigh number, these include cases of pure conduction, steady convective flow and Lorenz-like chaotic flow. Numerical results for the velocity and temperature fields are presented in order to characterize and quantify the different steady and unsteady 3-D flow regimes; the temporal evolution of the mass flow rate is also reported. Particular emphasis is placed upon the analysis of the unsteady convection flow regime.

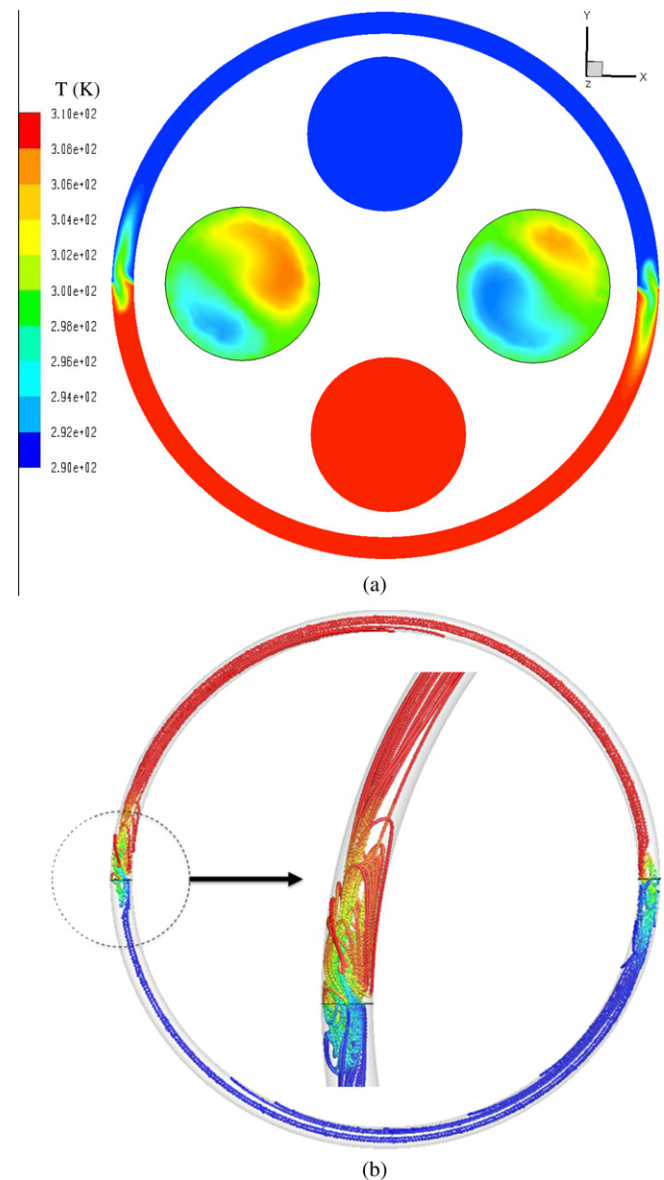


Fig. 4. Visualizations of steady state temperature and flow fields for $Ra = 25,000$. (a) Temperature fields in the midplane of the loop and in “four” selected cross sections around the loop. The thermal fields at $\theta = \pm\pi/2$ confirms the dominance of conduction over convection. (b) Streamline plot with a magnified view of the recirculation zone.

3.1. Steady convection regime

We first consider ranges of Rayleigh numbers that result in steady-state convection patterns, as this represents the most basic flow state. At the lowest Rayleigh numbers, the convection pattern is very weak and consists essentially of small, counter-rotating cells. The circulations are limited to the regions near the locations of the thermal boundary condition discontinuities (i.e., at $\theta = 0, \pi$); the remaining regions of the loop are motionless. This flow state corresponding to $Ra = 25,000$ is represented in Fig. 3 in terms of distribution of temperature (left) and vorticity (right) fields. The contour plots correspond to the vertical mid-plane of the loop in the regions near the temperature discontinuity between the hot

and cold walls. The isotherms show a dominant conductive mode, with hot fluid trapped in the lower half, and cold fluid in the upper half. The convective motion is oriented upward on the left and downward on the right, indicating that the fluid will circulate clockwise (CW) at a relatively higher Rayleigh number. Additional views of the thermal and flow structures are presented in Fig. 4a and b, respectively for this same low value of Ra . In Fig. 4a, the temperature fields at $\theta = -\pi/2$ and $\theta = \pi/2$ confirm that only conduction heat transfer is present. Near the boundary thermal discontinuities, asymmetric temperature distributions are observed in the horizontal cross sections, with the bulk of the fluid rising at $\theta = \pi$, and sinking at $\theta = 0$. A small recirculating region results in a steady local flow reversal on the left ($\theta = \pi$) and right ($\theta = 0$), as is clearly seen in the streamlines of Fig. 4b. It was found in a previous 2-D study conducted by the authors [22] at this value of Ra ,

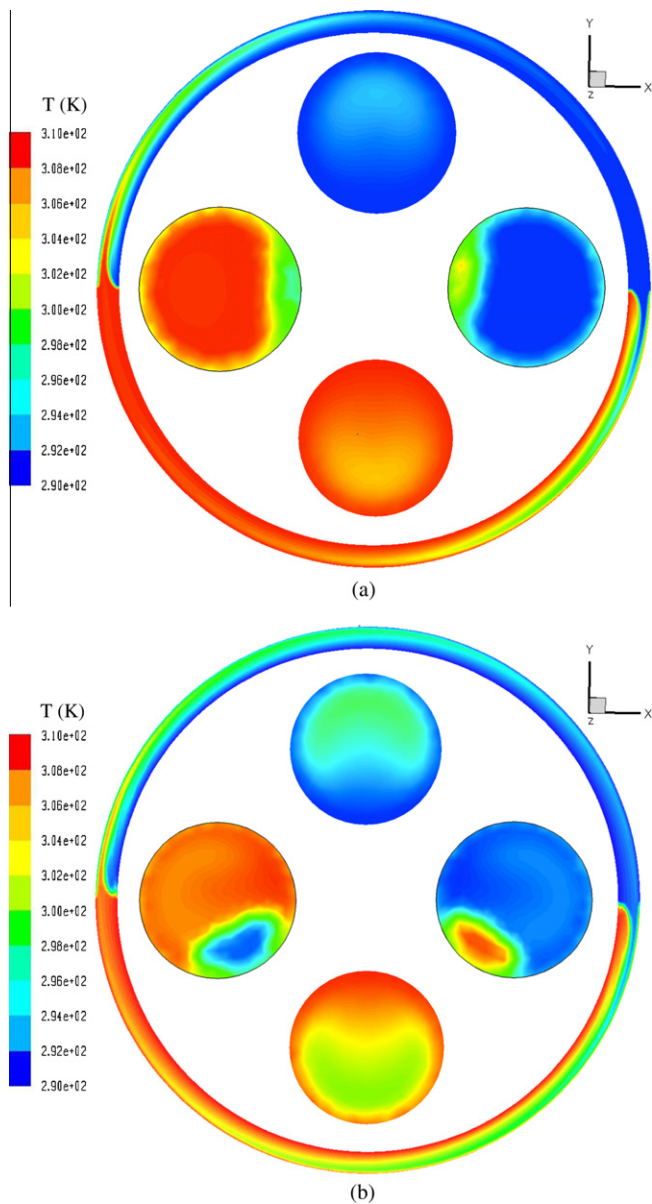


Fig. 5. Temperature distributions at four cross sections along the loop during the steady convection regime: (a) $Ra = 80,000$ and (b) $Ra = 800,000$. Isolated regions of stagnant fluid are formed in the inner sides of the loop at $\theta = \pi$ and $\theta = 0$. The thermal fields at $Ra = 800,000$ show the existence of two fluid “pockets” near the boundary discontinuities. Fluid temperatures within these pockets are either much lower or much higher than the main flow. These pockets traverse the loop in a vortical circulation and will create instabilities that lead the flow to oscillate at higher Ra .

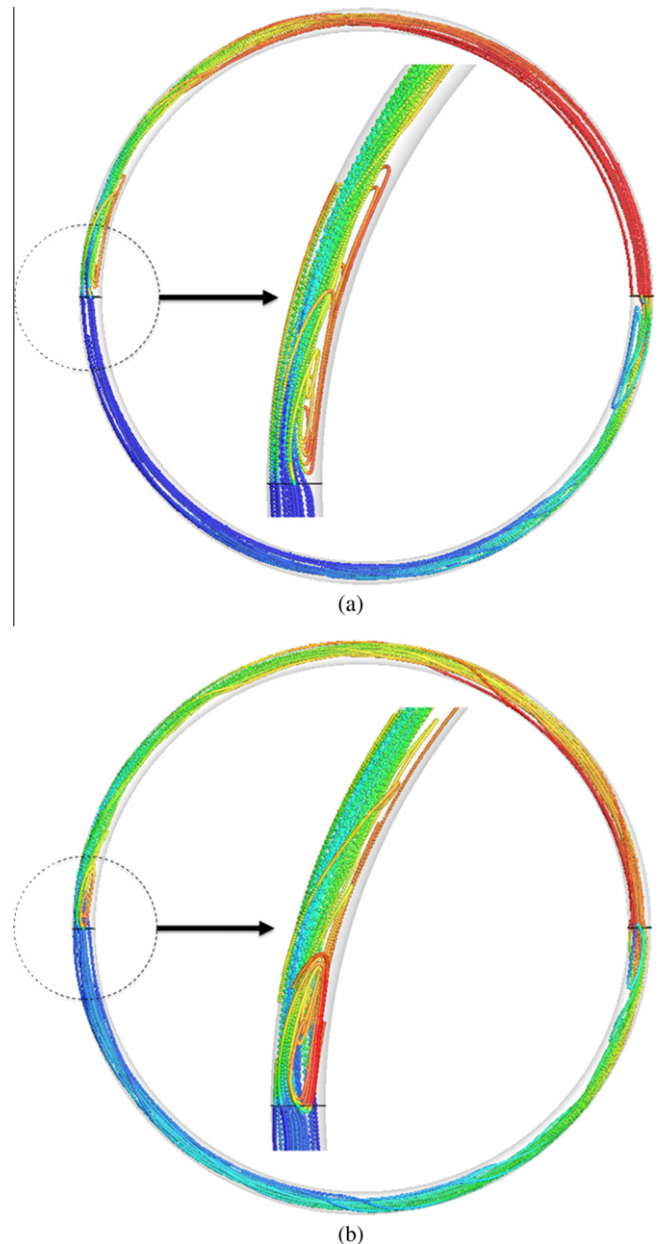


Fig. 6. Streamline visualizations of the flow field corresponding to Rayleigh numbers of (a) $Ra = 80,000$ and (b) $Ra = 800,000$. The lateral extent of the recirculation zone is compressed and the helicity of the re-circulating flow increases with Rayleigh number.

that a steady circulation pattern with relatively high velocities exists throughout the loop. This underscores the significance of 3-D effects by way of increased hydrodynamic resistance to initiating the flow in a 3-D geometry compared to a 2-D geometry.

When increasing Ra gradually from $Ra = 25,000$, the convective motion at the discontinuities intensifies, improving the overall contribution of convection to the global heat transfer through the loop. Above a certain critical value of Ra (around 45,000), a CW circulation along the loop becomes steady. This new state at the critical value of Ra may also rotate counter clockwise (CCW); the particular direction of the rotation is dictated by minute numerical asymmetries present in the initial condition of the numerical sim-

ulation. Fig. 5 illustrates the characteristics of the steady circulation state in terms of the temperature distribution at four cross sections along the loop at Rayleigh numbers of 80,000 and 800,000. Corresponding streamline visualizations for these cases appear in Fig. 6.

For $Ra = 80,000$, the steady circulation within the loop is evident when examining the temperature distributions within the four cross-sections. At the bottom of the loop, there is a slightly cooler core resulting from the clockwise flow circulation bringing cooler fluid to this location; the converse situation occurs at the top of the loop. Note that this “core” is not perfectly symmetric and in fact reverses its orientation between the top and the bottom. This is consistent with the temperature patterns observed in the cross-sections taken at the horizontal midplane of the loop. At these locations there is an isothermal core that occupies much of the cross section, whose temperature is more extreme than the surrounding boundary temperature. This is due to the velocities being greatest at these locations. However, there are also small isolated regions of stagnant fluid adjacent to the walls whose temperature nearly matches that of the boundary. Again there is an asymmetry in the location of these “pockets” on opposite sides of the horizontal midplane of the loop. Taken together, the temperature distributions at these four cross-sections indicate a vortical circulation pattern throughout the loop. This is strictly a three-dimensional ef-

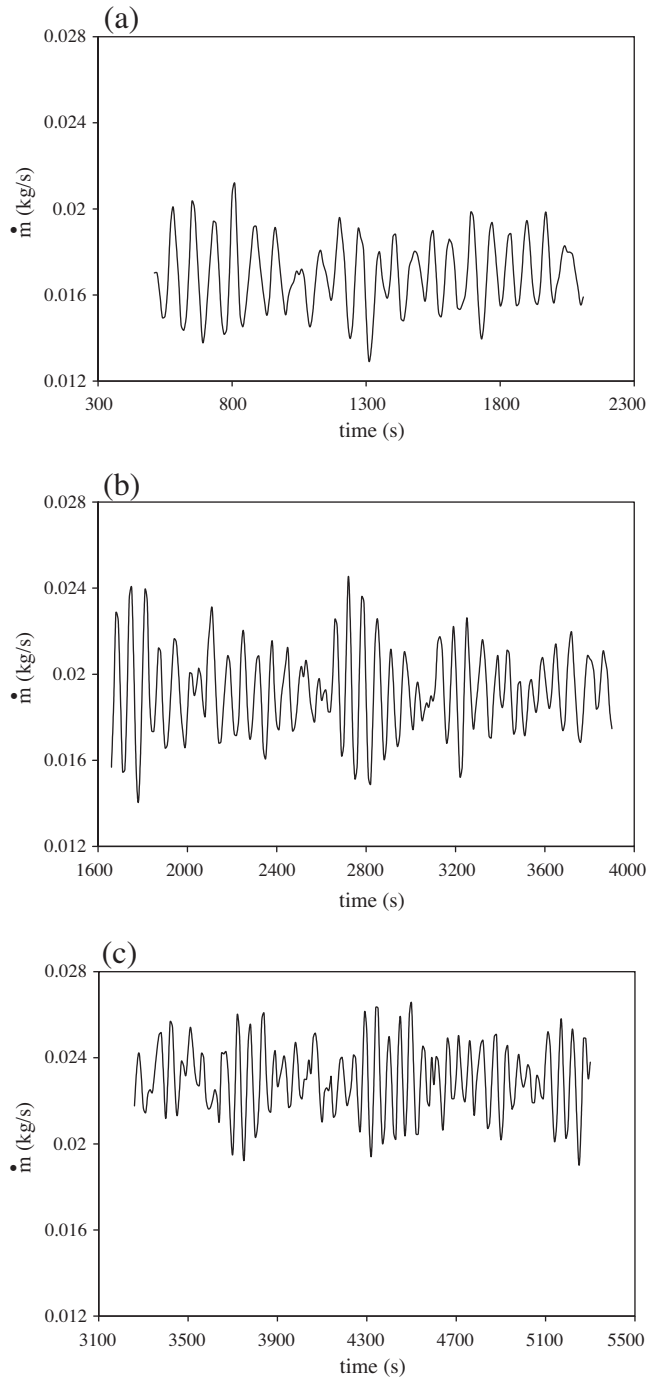


Fig. 7. Temporal evolution of the mass flow rate at different Rayleigh numbers of (a) 1.5×10^7 , (b) 2.02×10^7 and (c) 2.89×10^7 . The flow remains unidirectional, as the mass flow rate, \dot{m} , does not change sign.

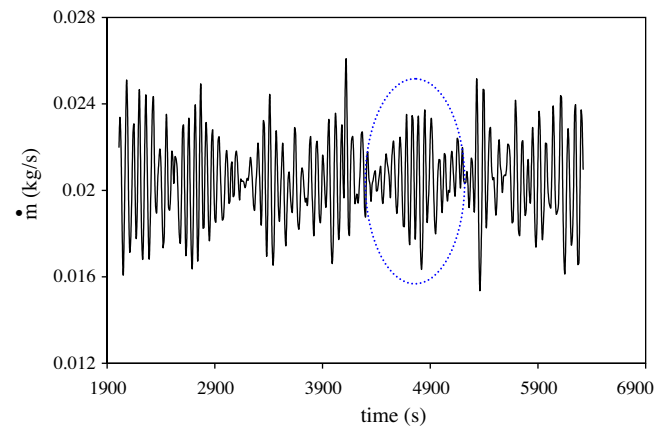


Fig. 8. Time history of the mass flow rate along the loop when the temperature difference $\Delta T = 40$ K ($Ra = 2.31 \times 10^7$). The flow oscillations show a unique beating pattern where the magnitude increases smoothly to reach a maximum and decreases again to become almost stable before the beginning of a new cycle.

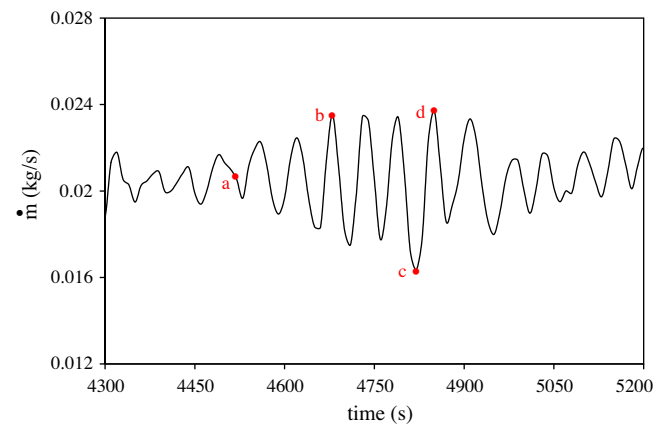


Fig. 9. A magnified view of the selected time window of Fig. 8 (dashed oval) showing more details of the flow regime. Oscillations of varying amplitude sharing the same period of approximately 70 s are observed.

fect and one that would not be observed in two-dimensional simulations.

As the Rayleigh number is increased to 800,000 one observes that these features become more pronounced. The overall circulation within the loop increases and, at the top and bottom of the loop, the result is a more extensive fluid core with a greater temperature differential with respect to the boundary. Meanwhile, in the horizontal midplane the aforementioned “pockets” increase in size and migrate to a different azimuthal location. There is also a marked variation in their temperature: the temperature within the pockets no longer matches the boundary value but rather inversions of the core temperatures. This behavior is intimately linked with the enhancement of the three-dimensional flow structures in these regions.

The streamline patterns at increasing Rayleigh numbers indicate two essential modifications of the flow structure when compared to the patterns observed at the much lower values. First, recirculation zones remain present at the $\theta = 0, \pi$ positions, the lateral extent of the zone is seen to be compressed to a greater extent by the circulating flow. This is evidently linked to the greater flow inertia at the increased Rayleigh numbers. Second, the interaction of the circulating and re-circulating flows at these locations leads to the development of a helical structure to the circulating flow in the remainder of the loop; this helical component is readily seen in Fig. 6. As Rayleigh number is further increased, these flow structures ultimately lead to hydrodynamic instabilities that result in a transition from a steady circulation pattern to an unsteady, oscillatory one. This regime is discussed in the next section.

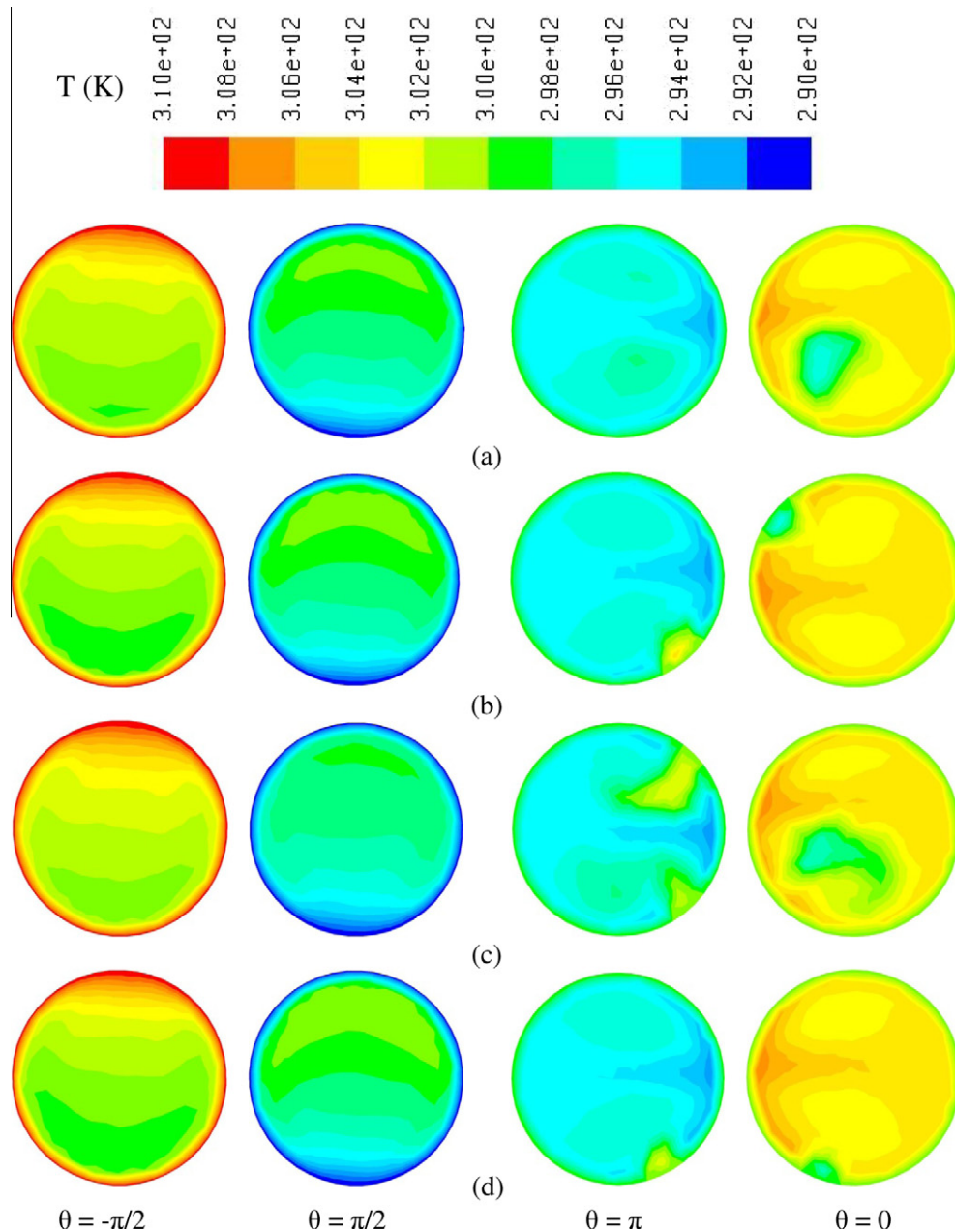


Fig. 10. Temporal evolution of the flow structure over one cycle of oscillations. Isotherms are plotted at selected times corresponding to instants a–d in Fig. 9. Minor qualitative changes are observed over time in the upper and lower regions of the loop. However, in the vicinity of the discontinuities at $\theta = \pi$ and $\theta = 0$ the flow is unstable and consists of two counter rotating vortices surrounded by a thin fluid layer either much hotter or cooler than the main vortices.

3.2. Unsteady convection regime

The numerical simulations reveal that a stable, steady convective circulation pattern persists and increases in strength until a threshold value of the Rayleigh number is reached. In this study, this value is found to be approximately 1.5×10^6 . Above this value the convective motion becomes unstable and transitions to an oscillatory pattern that fluctuates about some mean value; however, there is no reversal in the overall circulation pattern and the bulk flow remains unidirectional. The flow remains fully laminar and this state of seemingly random fluctuations in time is regarded as “chaotic convection”. The nature of the oscillations is depicted in Fig. 7 by the temporal evolution of the mass flow rate at different values of the Rayleigh number of 1.5×10^7 , 2.02×10^7 and 2.89×10^7 . We kept the ordinate-axis the same in all the figures to observe the changes in the mass flow rate amplitude as the Rayleigh number increases. The time window is not consistent as the objective here is limited to the visualization of the oscillation behavior at each Rayleigh number. Again, the bulk motion of the fluid is unidirectional – hence the mass flow rate never changes sign –, although local flow reversals are present as in the steady cases at the lower Rayleigh numbers. Overall, as the Rayleigh number is increased, the mean value of the mass flow rate is also increased as would be expected by the greater buoyant forcing. Furthermore, there is an accompanying increase in the amplitude of the fluctuations. Close inspection of the plots of mass flow rate reveals a sequence of fluctuations of relatively high amplitude followed by periods of relatively weak fluctuations where the fluid enters a temporary, quasi-stable state. To verify that the fluctuations in the mass flow rate were sustained – and not a transient phenomena, all simulations were performed for an extended duration of 2×10^4 sec (5.5 h) and no re-stabilization was observed.

To analyze the unsteady behavior in greater detail, we select a particular value of the Rayleigh number ($Ra = 2.31 \times 10^7$) corresponding to a temperature difference ΔT of 40 K. Fig. 8 shows the time history of the mass flow rate along the loop. For comparison purposes against the data displayed in Fig. 7, the scale of the ordinate-axis was kept the same. At this particular forcing, the flow oscillations show a unique beating pattern where the magnitude increases smoothly with time to reach a maximum and decreases again to become almost stable at an average value of about 0.021 kg/s. These patterns prevail in time despite variations in magnitude and oscillation period observed from one cycle to another. For a better understanding of the flow behavior during the chaotic regime, we focused our attention on the selected cycle shown in Fig. 8 (indicated by the dashed oval); this window of time is displayed in Fig. 9. More details can be extracted from this zoomed-in image including the oscillation period of approximately 70 s.

The flow visualization over the selected cycle of Fig. 8 is presented in Fig. 10. Isotherms are plotted at selected times corresponding to instants a–d in Fig. 9. These instants were chosen based on their corresponding \dot{m} magnitude to show typical flow structures occurring in the loop during one cycle of oscillations. Minor qualitative changes are observed over time in the upper and lower regions of the loop presented by the images at $\theta = -\pi/2$ and $\theta = \pi/2$. The temperature distribution in these locations indicates a large isothermal core with sharp gradients near the walls. In the vicinity of the discontinuities at $\theta = \pi$ and $\theta = 0$ the flow is unstable and consists of two counter rotating vortices. At $\theta = 0$ the vortices circulate warm fluid in the central region surrounded by a cold boundary layer. The cold pocket in Fig. 10b ($\theta = 0$) grows over time and moves around the surface before getting absorbed by one of the main vortices. These main vortices change in size and interestingly the cold pocket always forms attached to the larger vortex. A similar sequence of events occurs at the other discontinuity at $\theta = \pi$. To further correlate the observed thermal behavior

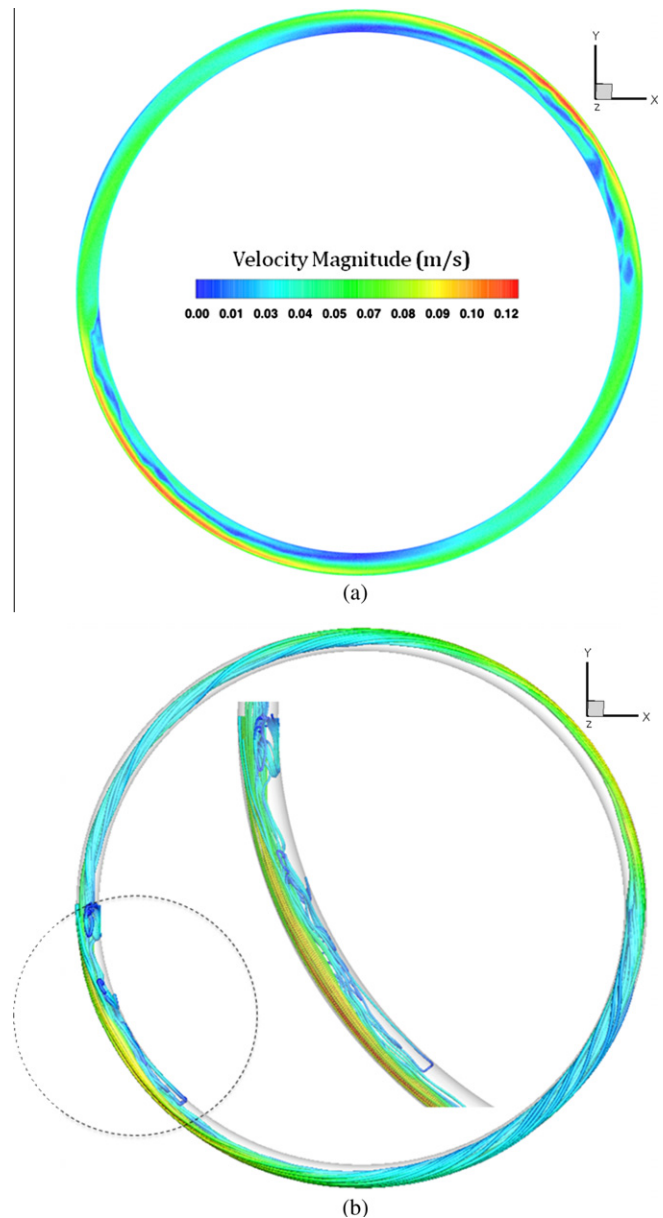


Fig. 11. Visualization of the instantaneous flow field corresponding to point “d” of Fig. 9. (a) Plot of the instantaneous velocity magnitude in the loop mid-plane. (b) Plot of the instantaneous streamlines. The vertical motion within the isolated recirculation zones is highly complex.

with the flow patterns, plots of the mid-plane velocity magnitude along with the instantaneous streamline pattern appear in Fig. 11 (a) and (b), respectively for the instant “d” identified in Fig. 9. The asymmetry of the flow field along the loop is clearly evident. Although there are sizable recirculation zones centered approximately at the $\theta = \pi/4$ and $-3\pi/2$ positions along the loop (antipodal points) these zones do not share the symmetry observed for the steady convection patterns. Within these zones the vortical motion is quite complicated. Also noteworthy is the high degree of helical motion that is present throughout the entire loop.

To identify the dynamical regimes occurring in the loop at ΔT of 40 K, we proceeded to a spectral analysis of the mass flow rate $\dot{m}(t)$ signal displayed in Fig. 8, the outcome is shown in Fig. 12. It is clear that the system response is a multi-period signal of frequencies varying in the interval 0.01–0.02 Hz. In fact the power spectrum peaks at a frequency $f_0 = 0.014$ surrounded by a sequence of secondary peaks of small magnitude.

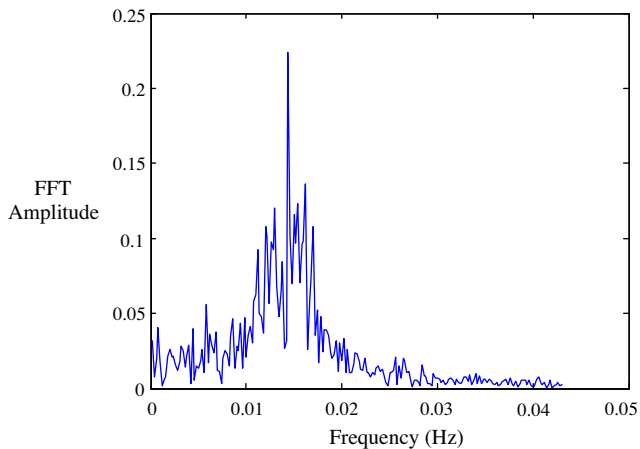


Fig. 12. Level of the mass flow rate signal displayed in Fig. 8. It is observed that this signal has multiple periods with frequencies varying in the interval between 0.01 and 0.02 Hz. The main peak occurs at a frequency $f_0 = 0.014$ (70 s) surrounded by a sequence of secondary peaks of small magnitude.

4. Conclusions

Three-dimensional numerical results of laminar natural convection inside a thermal convection loop filled with water, heated from below and cooled from above are presented. The equations of mass, momentum, and energy were solved using the finite-volume method. Unsteady numerical simulations were conducted fixing the Prandtl number at 5.83 and varying the Rayleigh number from 10^3 to 2.6×10^7 . Under these conditions, multiple flow regimes including conduction, steady convection, and unsteady convection were encountered in the loop as the Rayleigh number was increased.

It was found that the onset of convection originated at the discontinuities between the hot and cold walls and took the form of small vortices, while the remaining fluid along the loop was still motionless. These vortices intensified as Ra was increased and resulted in a steady fluid circulation that may rotate CW or CCW by chance. This new state appeared and became stable as long as Ra remained within the interval from 5×10^4 to 1.5×10^6 . However, starting at Ra of 8×10^5 , the flow visualization showed the appearance of two fluid pockets at the discontinuities, with temperatures that were either much lower or much higher than the main flow. These pockets created instabilities that led the flow to oscillate at higher Rayleigh numbers. Above Ra of 1.5×10^6 , the convective motion became oscillatory and any increase in Ra resulted in stronger oscillations. The flow oscillations showed a unique beating pattern at a particular value of Ra = 2.31×10^7 , which was equivalent to ΔT of 40 K. The flow visualization during one cycle of oscillations, presented by the temperature distribution at selected location within the loop, showed that minor qualitative changes were observed over time in the upper and lower regions of the loop. However, in the vicinity of the discontinuities at $\theta = \pi$ and $\theta = 0$ the flow is unstable and consists of two counter rotating vortices surrounded by a thin layer that was either much cooler or hotter than the main flow. These main vortices were highly unstable and changed size throughout the oscillation cycle. In agreement with the results found by Lavine et al. [5], the three dimensional flow structures increased the flow resistance, and dampened the flow instability mechanism responsible for bulk flow reversals observed in lower dimensional theoretical models and simulations. The exact details describing the mechanism by which this damping occurs are not clear.

In summary, the simulations reveal a highly complex and three-dimensional flow behavior within the loop characterized by localized recirculation zones and helical motion of the bulk circulation, the degree of which increases with Rayleigh number. These visualizations underscore the need for fully three-dimensional simulations to capture the detailed behavior of the toroidal convection loop phenomena.

Acknowledgments

The authors thank Kameron Decker Harris, Floyd Vilmont and Sarah Iams for helpful discussions during the course of this study. This project was supported jointly by the Vermont Advanced Computing Center (VACC), NSF-DMS Grant Number 0940271, and by NASA via Vermont Space Grant # NNG05GH16H.

References

- [1] A. Mertol, R. Greif, A Review of Natural Circulation Loops, in: S. Kakac et al. (Eds.), Handbook of Natural Convection: Fundamentals and Applications, Hemisphere, Washington, D.C, 1985, pp. 1033–1071.
- [2] R. Greif, Natural circulation loops, ASME J. Heat Transfer 110 (1988) 1243–1258.
- [3] P. Welander, On the oscillatory instability of a differentially heated fluid loop, J. Fluid Mech. 29 (1967) 17–30.
- [4] H.F. Creveling, J.F. De Paz, J.Y. Baladi, R.J. Schoenhals, Stability characteristics of a single-phase free convection loop, J. Fluid Mech. 67 (1975) 65–84.
- [5] A.S. Lavine, R. Greif, J.A.C. Humphrey, Three-dimensional analysis of natural convection in a toroidal loop: effect of tilt angle, ASME J. Heat Transfer 108 (1986) 796–805.
- [6] A.S. Lavine, R. Greif, J.A.C. Humphrey, A three-dimensional analysis of natural convection in a toroidal loop – the effect of Grashof number, Int. J. Heat Mass Transfer 30 (1987) 251–262.
- [7] E.A. Burroughs, E.A. Coutsias, L.A. Romero, A reduced-order partial differential equation model for the flow in a thermosyphon, J. Fluid Mech. 543 (2005) 203–237.
- [8] G. Desrayaud, A. Fichera, M. Marcoux, Numerical investigation of natural convection in a 2D-annular closed-loop thermosyphon, Int. J. Heat Fluid Flow 27 (2006) 154–166.
- [9] E.N. Lorenz, Deterministic nonperiodic flow, J. Atmos. Sci. 20 (1963) 130–141.
- [10] J.B. Keller, Periodic oscillations in a model of thermal convection, J. Fluid Mech. 26 (1966) 599–606.
- [11] M. Gorman, P.J. Widmann, K.A. Robins, Nonlinear dynamics of a convection loop: a quantitative comparison of experiment with theory, Physica D 19 (1986) 255–267.
- [12] P.K. Yuen, H.H. Bau, Optimal and adaptive control of chaotic convection - theory and experiments, Phys. Fluids 11 (1999) 1435–1448.
- [13] J. Tang, H.H. Bau, Stabilization of the no-motion state in Rayleigh–Bénard convection through the use of feedback control, Phys. Rev. Lett. 70 (1993) 1795–1798.
- [14] J. Tang, H.H. Bau, Feedback control stabilization of the no-motion state of a fluid confined in a horizontal, porous layer heated from below, J. Fluid Mech. 257 (1993) 485–505.
- [15] J. Tang, H.H. Bau, Stabilization of the no-motion state of a horizontal fluid layer heated from below with Joule heating, ASME J. Heat Transfer 117 (1995) 329–333.
- [16] J. Tang, H.H. Bau, Experiments on the stabilization of the no-motion state of a fluid layer heated from below and cooled from above, J. Fluid Mech. 363 (1998) 153–171.
- [17] J. Tang, H.H. Bau, Numerical investigation on the stabilization of the no-motion state of a fluid layer heated from below and cooled from above, Phys. Fluids 10 (1998) 1597–1610.
- [18] P.K. Vijayan, H. Austregesilo, Scaling laws for single-phase natural circulation loops, Nucl. Eng. Des. 152 (1994) 331–347.
- [19] P.K. Vijayan, Experimental observations on the general trends of the steady state stability behavior of single-phase natural circulation loops, Nucl. Eng. Des. 215 (2002) 139–152.
- [20] Y.Y. Jiang, M. Shoji, M. Naruse, Boundary condition effects on flow stability in a toroidal thermosyphon, Int. J. Heat Fluid Flow 23 (2002) 81–91.
- [21] Y.Y. Jiang, M. Shoji, Spatial and temporal stabilities of flow in a natural circulation loop: influences of thermal boundary condition, ASME J. Heat Transfer 125 (2003) 612–623.
- [22] E.H. Ridouane, C.M. Danforth, D.L. Hitt, A 2-D numerical study of chaotic flow in a natural convection loop, Int. J. Heat Mass Transfer 53 (2010) 76–84.
- [23] FLUENT Manual, FLUENT Inc., 10 Cavendish Court, Centerra Resource Park, Lebanon, NH 03766, USA, 2006.